Excited-state electronic coherence in vinyl bromide ions

Hongbo Du
Department of Physics and Astronomy, Vanderbilt University, Nashville, Tennessee 37235, USA
and Department of Physics, School of Science, Xi'an Technological University, Xi'an, Shaanxi 710032, China

Cody Covington*
Department of Physics and Astronomy, Vanderbilt University, Nashville, Tennessee 37235, USA
and Department of Chemistry, Austin Peay State University, Clarksville, Tennessee 37044, USA

Stephen R. Leone†
Chemical Sciences Division, Lawrence Berkeley National Laboratory, Berkeley, California 94720, USA;
Department of Chemistry, University of California, Berkeley, California 94720, USA;
and Department of Physics, University of California, Berkeley, California 94720, USA

Kálmán Varga‡
Department of Physics and Astronomy, Vanderbilt University, Nashville, Tennessee 37235, USA

(Received 7 August 2019; published 20 November 2019)

We have performed time-dependent density functional theory calculations on the molecule vinyl bromide under ionization by a laser and have found long-lived coherent oscillations in the electron density created by a superposition of orbitals. The superposition of the molecular orbitals is quite pronounced for some intensities and is compared to varied alignments and strengths of the exciting laser. The coherence between the orbitals is also shown to be strongly dependent upon atomic motion.

DOI: 10.1103/PhysRevA.100.053412

I. INTRODUCTION

The rapid development of ultrafast laser pulses has enabled the investigation of coherent electron excitations and charge migration dynamics [1–8]. Coherence is best described by using the density matrix formalism which is a very powerful tool to study the statistical distribution of quantum states of a system. Coherence between quantum states is characterized by nonzero off-diagonal elements of the density matrix. Coherent states [9], especially those with a long lifetime, play a very important role in many physical processes, including energy transfer [10], photosynthesis [11,12], quantum computation [13,14], observation of electron dynamics [5], high harmonics interferometry [15], and charge migration [1].

Ultrashort laser pulses can generate coherent vibrational [16,17] or electronic wave packets [5,18]. Coherent electron motion has been intensively studied in atoms [5,19], for example, strong coherence is observed between $^3P_2^0$-$^3P_0^0$ of Xe^{2+} [18] showing the possibility for selective preparation of coherent electron dynamics. This electron dynamics is much faster than the nuclear motion and it may be used to steer charge migration [20] and the accompanying bond rearrangement processes in molecules.

Coherent state preparation by strong-field ionization has been studied theoretically for atoms [21,22] and molecules [2,23–28]. Time-dependent multichannel theory has been used [22,29] to study the coherence of quantum states after strong-field ionization in noble-gas atoms. Small molecules, where the nuclear motion becomes important, have also been studied [27,30]. Theoretical studies envisioning the possibility of probing coherent states in complex molecules have also been pursued [23,24,31]. The multiconfigurational time-dependent Hartree (MCTDH) method [27] and the time-dependent density functional theory (TDDFT) [23,24,31] are the most popular computational approaches to study the electron dynamics after ionization. The MCTDH method uses full nuclear quantum dynamics, but it is limited by the computational cost and the requirement of an *a priori* knowledge of the potential-energy surfaces. In TDDFT, the electrons are treated quantum mechanically, but the nuclei follow classical trajectories based on the Ehrenfest dynamics.

The role of nuclear dynamics in the electronic decoherence has received particular attention in theoretical studies [22,27,28,32]. First it was assumed that the nuclear motion is slow and can be neglected, but later it was realized that [33] the charge migration can induce an ultrafast nuclear response. The question then is how long the electronic coherence can survive the effect of the nuclear motion. Polyatomic molecules (e.g., paraxylene and phenylalenine) were studied in a full quantum mechanical treatment of electron and nuclear dynamics [27,28] and it was found that the electronic coherence

*cody.l.covington@vanderbilt.edu
†srl@berkeley.edu
‡kalman.varga@vanderbilt.edu

is dephased on a timescale of a few femtoseconds. A recent full quantum dynamical study [26] simulated the charge migration in propiolic acid, showing charge oscillation between the carbon triple bond and the carbonyl oxygen lasting for about 10 fs before decaying due to the nuclear motion.

In this work, we will investigate a different candidate for a molecule where electronic coherence can persist for long timescales. Vinyl bromide, C_2H_3Br, ion has several low-lying electronically excited states, providing access to both electronic and vibrational coherent dynamics following strong-field ionization. The molecule has two distinct parts, i.e., the bromine atom and the carbon-hydrogen (ethylenyl) fragment, and the molecular orbitals can be localized on either part. The coherent excitation of these orbitals leads to charge migration between the two parts of the molecule forming coherent oscillations of the electron density.

Time-dependent density functional theory calculations will be used [34] to study the ionization and the subsequent electron and nuclear dynamics of the molecule caused by a short, strong laser pulse. The nuclear motion will be described using the Ehrenfest dynamics. The full quantum nuclear dynamics used in the MCTDH method is limited to a short timescale and, in this work, we would like to simulate the system up to few-hundred femtoseconds. Unlike previous works that studied the dynamics after ionization, we use a laser field to ionize the molecule and the system with multiple partially ionized orbitals is studied. To study the effect of laser parameters, several different wavelengths, pulse fields, and laser polarization alignments will be used.

II. COMPUTATIONAL DETAILS

The electron dynamics is described in the framework of TDDFT [34] using a real-space grid with real-time propagation. This formalism was previously used by our group to describe Coulomb explosion of molecules [35–37], electron dynamics in graphene and silicon subject to intense laser pulses [38–40], and high-energy irradiation of materials [41,42].

At the beginning of the TDDFT calculations, the system is initialized by calculating the ground state by a density functional theory calculation. After that, the time-dependent Kohn-Sham orbitals, $\psi_k(\mathbf{r},t)$, are determined by solving the time-dependent Kohn-Sham equation,

$$i\hbar\frac{\partial\psi_k(\mathbf{r},t)}{\partial t} = H\psi_k(\mathbf{r},t), \tag{1}$$

where k is a quantum number labeling the orbital. The Hamiltonian is given by

$$H = -\frac{\hbar^2}{2m}\nabla_{\mathbf{r}}^2 + V_{\mathrm{H}}[\rho](\mathbf{r},t) + V_{\mathrm{XC}}[\rho](\mathbf{r},t) + V_{\mathrm{ext}}(\mathbf{r},t), \tag{2}$$

where ρ denotes the electron density, which is defined by a sum over all occupied orbitals,

$$\rho(\mathbf{r},t) = \sum_{k=1}^{\infty} o_k|\psi_k(\mathbf{r},t)|^2. \tag{3}$$

The factor of o_k is the occupation of the orbital (typically 2), V_{H} is the Hartree potential, defined by

$$V_{\mathrm{H}}(\mathbf{r},t) = \int d\mathbf{r}'\frac{\rho(\mathbf{r}',t)}{|\mathbf{r}-\mathbf{r}'|}, \tag{4}$$

and V_{XC} is the exchange-correlation potential. This functional was approximated by the adiabatic local-density approximation (ALDA) with the parametrization of Perdew and Zunger [43]. The last term in Eq. (2), V_{ext}, is the external potential, which includes the implicitly time-dependent potential due to the ions, V_{ion}, and the explicitly time-dependent potential due to the electric field of the laser, V_{laser}. V_{ion} is a sum of norm-conserving pseudopotentials of the form given by Troullier and Martins [44] centered at each ion.

V_{laser} is described using the dipole approximation, $V_{\mathrm{laser}} = \mathbf{r}\cdot\mathbf{E}(t)$, with the time-dependent electric field given by

$$\mathbf{E}(t) = E_{\max}\exp\left[-\frac{(t-t_0)^2}{2a^2}\right]\hat{\mathbf{k}}\sin[\omega(t-t_0)]. \tag{5}$$

The parameters a, t_0, and $E_{\max}$ define the width, initial position of the center, and the maximum amplitude of the Gaussian envelope, ω describes the frequency of the laser, and $\hat{\mathbf{k}}$ is the direction of the electric field.

In our calculations, the time-dependent orbitals are propagated using a fourth-order Taylor expansion of the propagator [45–49], so that the propagation of the Kohn-Sham orbitals over a very short time step, δt, is given by

$$\psi_k(\mathbf{r},t_q+\delta t) \approx \sum_{n=0}^{4}\frac{1}{n!}\left[-\frac{i\delta t}{\hbar}H(\mathbf{r},t_q)\right]^n\psi_k(\mathbf{r},t_q). \tag{6}$$

The operator is applied for N time steps until the final time, $t_{\mathrm{final}} = N\delta t$, is obtained. While the Taylor propagation is not unconditionally stable, for time steps chosen to be suitably small, the propagation is very accurate. The advantage of the Taylor propagation is that its simple form only requires the repeated action of the Hamiltonian on the wave function. A review and comparison of the advantages and disadvantages of different time-propagating schemes in TDDFT can be found in Ref. [50].

In real-space TDDFT, the Kohn-Sham orbitals are represented at discrete points in real space. In practice, these discrete points are organized in a uniform rectangular grid and the accuracy of the simulations are controlled by adjusting a single parameter: the grid spacing. At the walls of the simulation cell, we enforce the boundary condition that the Kohn-Sham orbitals are zero at the walls. When a strong laser field is applied, ionization may occur and the zero-boundary condition can lead to an unphysical reflection of the wave function off the walls of the simulation cell. To prevent this reflection, we implemented the complex absorbing potential (CAP) of Ref. [51].

As the molecule is ionized by the laser field, electron density will travel to the edge of the simulation box where it is absorbed by the CAP. The total electron number,

$$N(t) = \int_V \rho(\mathbf{r},t)d^3x, \tag{7}$$

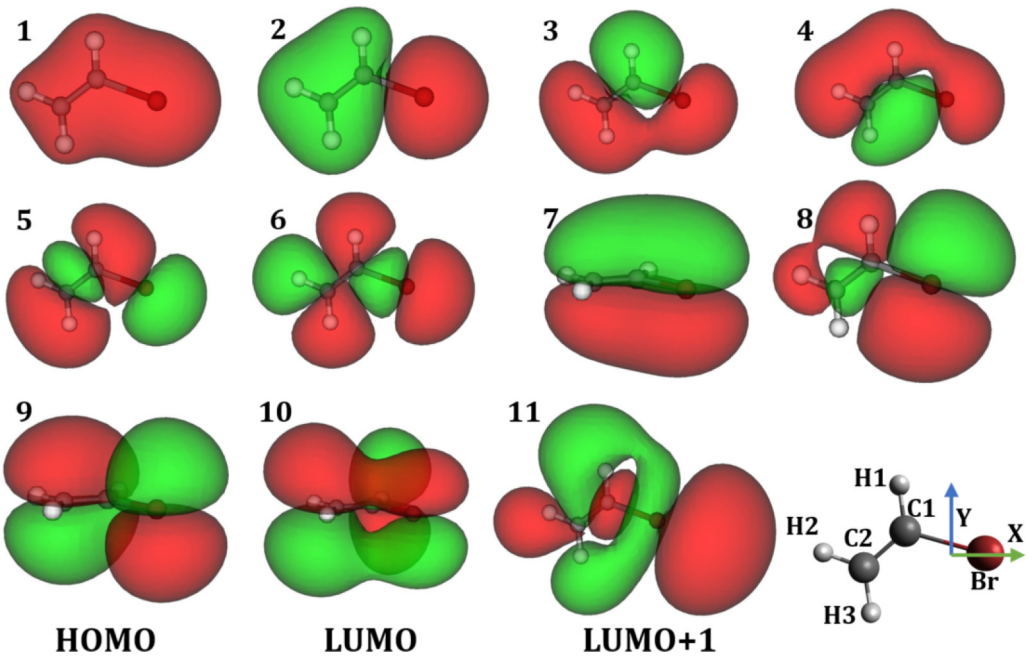

FIG. 1. Isosurfaces of Ψ values of 0.02 and −0.02 of the nine occupied and the lowest two unoccupied molecular orbitals of the vinyl bromide electronic ground state as a neutral molecule. On the first (lowest energy) orbital (upper left corner), the molecule lies in the *xy* plane and the atoms are numbered. This numbering will be used to define the relative motion between nuclei. Atomic positions, *x* and *y* axes, and system origin are shown on the bottom right. Note that orbitals 7, 9, and 10 are rotated about the *x* axis to show the node in the molecular plane.

where V is the volume of the simulation box, will therefore diverge from the initial electron number, $N(0)$. We interpret $N(0) - N(t)$ as the total ionization of the molecule.

The motion of the nuclei in the simulations is treated classically based on the Ehrenfest theorem. The quantum forces on the nuclei, which are due to the electrons, are given by the derivatives of the expectation value of the total electronic energy with respect to the ionic positions. These forces are then fed into Newton's Second Law, giving

$$M_i \frac{d^2\mathbf{R}_i}{dt^2} = Z_i \mathbf{E}_{\text{laser}}(t) + \sum_{j\neq i}^{N_{\text{ions}}} \frac{Z_i Z_j (\mathbf{R}_i - \mathbf{R}_j)}{|\mathbf{R}_i - \mathbf{R}_j|^3} - \nabla_{\mathbf{R}_i} \int V_{\text{ion}}(\mathbf{r}, \mathbf{R}_i)\rho(\mathbf{r}, t)d\mathbf{r}, \tag{8}$$

where M_i and Z_i are the mass and pseudocharge (valence) of the ith ion, respectively, and N_{ions} is the total number of ions.

The computational results presented in the next section use the following parameters. The rectangular box is given by $L_x = L_y = L_z = 24.24$ Å. The grid spacing is 0.24 Å in each direction. The CAP is nonzero in a region that is 5 Å from the walls of the simulation cell. The time step for the propagation of the wave function is $\delta t = 0.001$ fs. The equation of the nuclear motion [Eq. (8)] is solved with the Verlet algorithm with time step 0.004 fs. These parameters lead to very well-converged results.

The molecule is placed in the simulation box, as shown in Fig. 1. Figure 1 also shows the orbital densities of the occupied and the lowest two unoccupied orbitals.

To describe the coherence between the molecular electronic orbitals, we have defined the overlaps,

$$c_{ij}(t) = \langle \psi_i(t) | \psi_j(0) \rangle, \tag{9}$$

where $\psi_i(t)$ is the ith molecular orbital at time t and $\psi_j(0)$ is the ground-state Kohn-Sham orbital, which is the orbital that has been used to initialize the wave function. If a state i is a coherent superposition of two states j and k, then its time dependence can be described as

$$\psi_i(t) = c_{ij}(t)\psi_j(0) + c_{ik}(t)\psi_k(0). \tag{10}$$

In general,

$$\psi_i(t) = \sum_j c_{ij}(t)\psi_j(0), \tag{11}$$

where the summation is over the occupied and unoccupied states. In the present work, we only calculate the occupied ground-state orbitals and two of the lowest unoccupied orbitals, so Eq. (11) is not used to represent the wave function, and $\psi_i(t)$ is calculated by direct time propagation. The charge migration and coherence of the electronic states have often been described by superpositions such as in Eq. (10) [24,25,52–55].

We also define the sum of squares of the inner product,

$$C_i = \sum_{j\in\text{occupied}} |c_{ij}(t)|^2, \tag{12}$$

which shows what percentage of a given time-dependent wave function remains in the subspace spanned by the ground-state orbitals.

TABLE I. The ground-state orbital energies for vinyl bromide with the expectation values of x and y in units of Å. Orbital 8 (the HOMO-1) is located more on the bromine atom since the Br atom is towards the positive x axis, and orbital 9 (the HOMO) is located more on the C atoms. The orbitals are numbered by energy and the HOMO-X notation is also given.

Orbital	E (eV)	$\langle x \rangle$	$\langle y \rangle$
1 (HOMO-8)	−21.28	0.0092	0.0965
2 (HOMO-7)	−18.52	−1.1888	0.0172
3 (HOMO-6)	−14.29	−1.3195	0.1999
4 (HOMO-5)	−11.96	−1.5283	0.1604
5 (HOMO-4)	−10.97	−1.2103	−0.1617
6 (HOMO-3)	−9.12	−1.1686	−0.0119
7 (HOMO-2)	−8.72	−0.4755	0.1313
8 (HOMO-1)	−7.16	0.576	0.0021
9 (HOMO)	−6.49	−0.474	−0.0431
10 (LUMO)	−1.75	−1.4494	0.0201
11 (LUMO+1)	−1.06	0.3173	0.0199

Other quantities can also be used to describe coherence. Reference [23], for example, used the instantaneous ground-state Kohn-Sham orbitals (states obtained by diagonalizing the Kohn-Sham matrix at the same time frame) in place of $\psi_k(0)$ in Eq. (9). This only requires a diagonalization in their basis-function-based approach, but it would be very time consuming in our real-space basis case.

One should carefully interpret the results of the TDDFT calculations. Charge transfer and charge oscillations can be accurately describe by TDDFT provided that suitable exchange correlations are used, but for other quantities TDDFT may perform less reliably. Recent reviews on charge transfer and excitations [56–58] emphasize the challenges and limitations of applications of TDDFT.

III. RESULTS AND DISCUSSION

We will label orbitals by numbers from lowest energy to highest energy in ascending order. This is different from the highest occupied molecular orbital minus X (HOMO-X) notation that is typically used because we want to avoid labels such as HOMO-8, etc., especially in figures. Refer to Table I for the labeling of the orbitals in HOMO-X notation.

A. Laser fields and ionization

To study the dependence of the results on laser parameters [see Eq. (5)], three different laser pulses are used in the calculations:

(A) $E_{\max} = 1.4$ V/Å with wavelength 124 nm in the x direction, with parameters of $a = 1.38$ fs and $t_0 = 9$ fs. This corresponds approximately to a pulse intensity of 2.6×10^{13} W/cm^2 and a pulse duration of 4.5 fs. See Fig. 2(a) for the amplitude of the laser as a function of time.

(B) $E_{\max} = 1.5$ V/Å with wavelength 124 nm in the z direction, with parameters of $a = 1.38$ fs and $t_0 = 9$ fs. This corresponds approximately to a pulse intensity of 3.0×10^{13} W/cm^2 and a pulse duration of 4.5 fs.

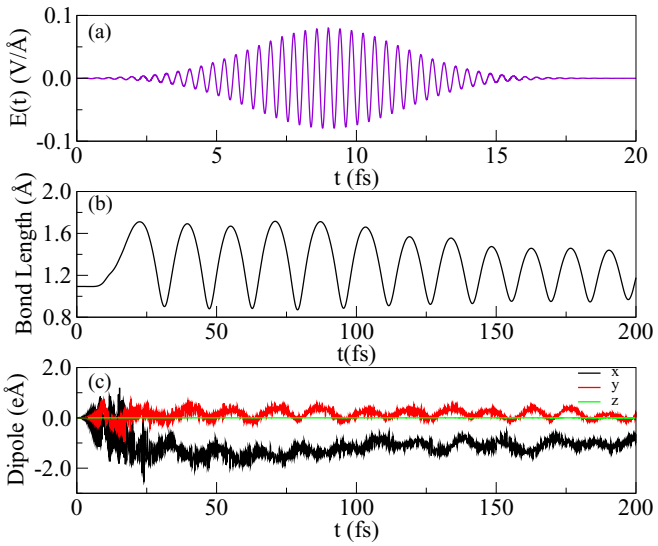

FIG. 2. (a) Laser pulse amplitude as a function of time. (b) The C1-H1 bond length. (c) Time-dependent dipole moments (in units of eÅ) for laser (A). The black, red, and green lines show the time dependence of the dipole moments in the x, y, and z directions.

(C) $E_{\max} = 5$ V/Å with wavelength 790 nm in the x direction, with parameters of $a = 1.38$ fs and $t_0 = 9$ fs. This corresponds approximately to a pulse intensity of 3.3×10^{14} W/cm^2 and a pulse duration of 4.5 fs.

The ionization energies of orbitals 9, 8, and 7 (the HOMO, HOMO-1, and HOMO-2 states) are experimentally determined to be around 10 eV [59], corresponding to photons of wavelength 124 nm, and that motivated the choice of the laser wavelength in the first two cases. Considering that TDDFT calculations using ALDA typically underestimate the ionization energies, this wavelength is just an approximation to the optimal one.

The third wavelength corresponds to the experimentally available Ti:sapphire laser. The pulse width and field strength were chosen to be short enough to not significantly interfere with the dynamics of the nuclei, but be strong enough to cause ionization.

The ionization during laser pulse (A) removes slightly less (5%) than two electrons from the molecule [see Fig. 3(c)]. By increasing the field strength to 1.5 eV, two electrons are removed but the molecule dissociates. Most of the ionization occurs during the interaction with the laser. Laser pulse (A) ionizes all orbitals, but most electron density is removed from orbital 8 [see Fig. 3(b)] and the next most ionized are orbitals 9 and 6. The orbital ionization mostly follows the orbital energy order, with a notable exception of orbitals 7 and 9. Laser (A) is parallel to the plane of the molecule and more easily removes electrons from orbital 8 (the HOMO-1 level) due to the symmetry of that orbital (see Fig. 1). During the laser pulse, orbitals 8 and 9 change order, and orbital 8 is slightly less bound than orbital 9, but later orbital 9 switches back to be the highest-energy orbital [Fig. 3(a)].

Figure 3(d) shows the bond lengths between the atoms as a function of time for laser (A). The bond lengths increase during the stage of strong ionization and continue to oscillate

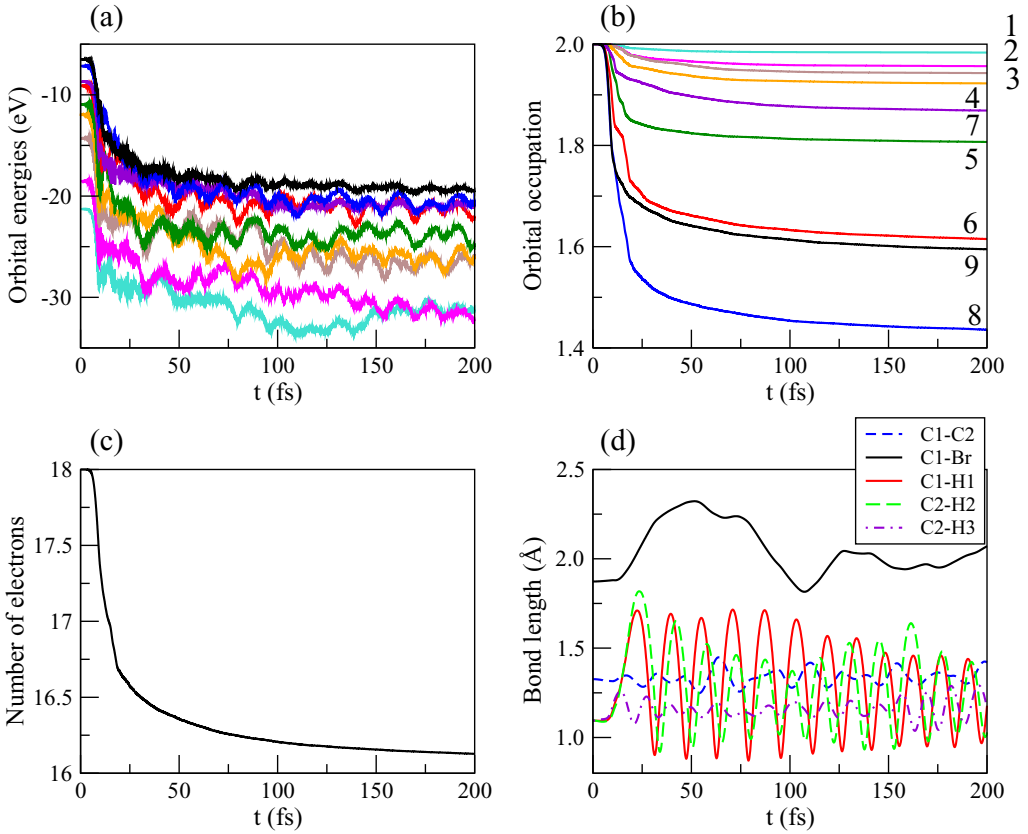

FIG. 3. (a) Orbital energies, (b) orbital occupation, (c) number of electrons, and (d) bond length between the atoms as a function of time for laser (A). (a) The HOMO is the highest curve (orbital 9) followed by the HOMO-1 (orbital 8), and so on. (b) The orbital indices are shown.

afterwards. This figure and later figures show that the amplitude of oscillation depends on the ionization, in particular it depends from which orbitals the electron density is removed.

The general behavior of orbital energies,

$$\langle\psi_k(t)|H|\psi_k(t)\rangle, \tag{13}$$

as a function of time, shown in Fig. 3(a), is governed by two factors. The long-term oscillations are due to the vibrational motion of the atoms. The period of these oscillations is very close to the period of the bond oscillations [Fig. 3(d)]. The short-term oscillations, which look like spikes on Fig. 3(a), are due to the laser excitation and the subsequent interaction between the electrons. Initially, the energy starts to oscillate due to the laser field and the period of oscillation is about the period of the laser, 0.4 fs. As the electrons interact, the oscillation becomes irregular and the minimum and maximum of the amplitude of oscillations follow each other on a roughly 0.1 fs timescale. This rapid oscillation will also show up in the time dependence of the overlaps, as we will show later.

Laser (B) is directed perpendicular to the molecular plane and mostly interacts with orbitals 9 and 7 (see Fig. 1). Consequently, it mostly ionizes these orbitals. As Fig. 5(c) shows, one electron is removed from the molecule, ionizing, only to some extent, orbital 7 and, to a lesser extent, orbital 8. The ionization of other states is minimal in this case [see Fig. 5(b)].

Calculations have also been performed using an exciting laser pulse more akin to those routinely used for experiments [laser (C)]. The results for these simulations can be seen in Fig. 6. Two electrons are removed from the molecule and ionization occurs from more orbitals than the other laser pulses, with orbitals 9, 6, 7, 4, 5, and 8 all being ionized to some extent.

B. Dipole moment

The time-dependent dipole moment of the vinyl bromide molecule subject to a laser pulse (A) is shown in Fig. 2(c). The ionization removes electrons from different orbitals, which are centered and localized at different atoms, changing the electron distribution of the molecule.

The initial change in dipole moment is due to the laser field drawing some electron density away from their ground-state distribution and then from the ionization caused by removing electron density from the orbitals. Table I shows the expectation value of the position operator for different orbitals in the ground state. From these values, one can estimate how the ionization of a given orbital contributes to the initial change in the dipole moment. Positive $\langle x\rangle$ values indicate that the orbital is localized more on the Br atom and negative values mean localization on the other side of the molecule (see Fig. 1 for the origin of the coordinate system).

During and immediately following the excitation by laser (A), there is a shift in the electron density towards the Br atom since orbital 8 was ionized most and it was located more on the Br atom. The Br atom is located in the positive x direction, which registers as a decrease in the x component of the dipole moment. The z component of the dipole moment

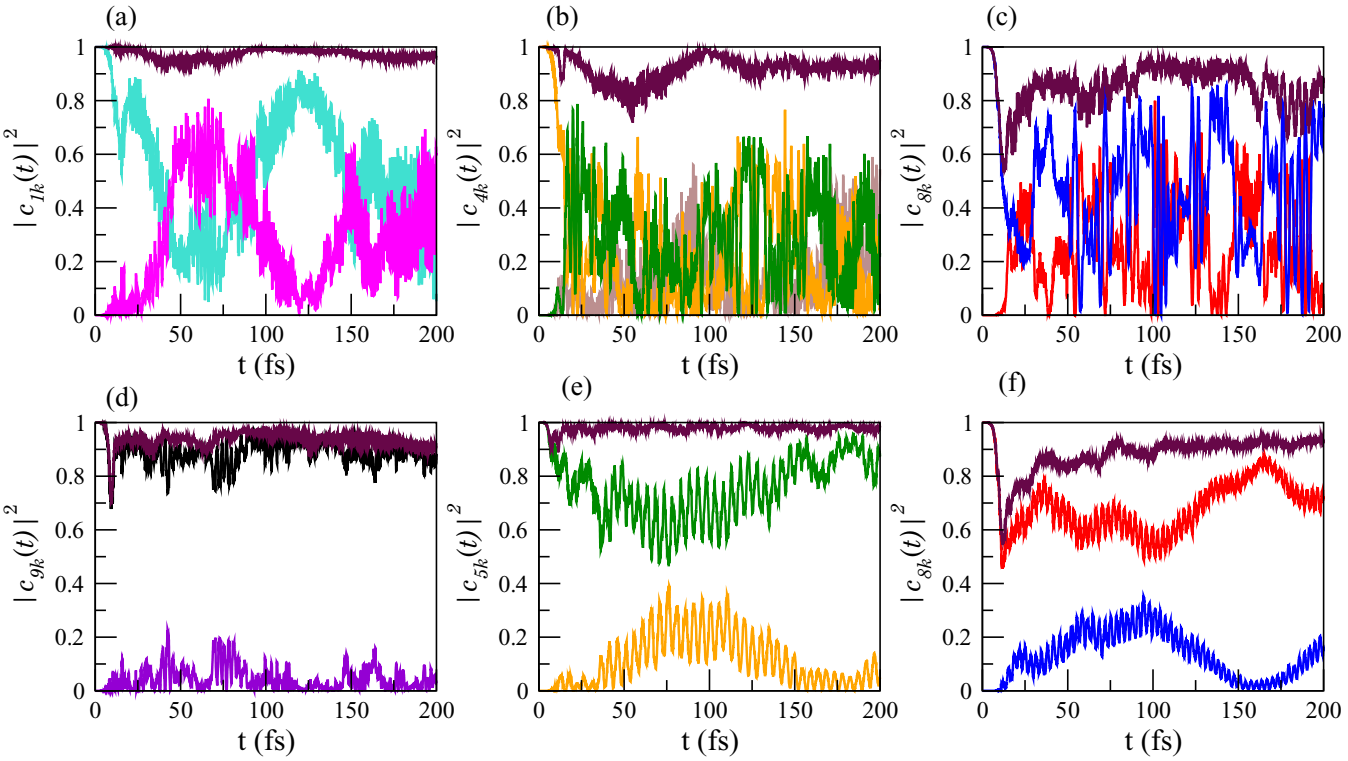

FIG. 4. Squared inner products as a function of time for laser (A). (a) $|c_{1k}(t)|^2$, $k = 1$ cyan line (starting in the left upper corner), $k = 2$ magenta line (starting at left bottom corner), and C_1 maroon line. (b) $|c_{4k}(t)|^2$, $k = 3$ brown line, $k = 4$ orange line (starting at the left upper corner), $k = 5$ green line (stating at the left bottom), and C_4 maroon line (upper curve). (c) $|c_{8k}(t)|^2$, $k = 6$ red line (starting at the left bottom), $k = 8$ blue line, and C_8 maroon line (upper curve). (d) $|c_{9k}(t)|^2$, $k = 7$ violet line (lowest curve), $k = 9$ black line, and C_9 maroon line (upper curve). (e) Fixed nuclei: $|c_{4k}(t)|^2$, $k = 3$ brown line (lower curve), $k = 4$ orange line, $k = 5$ green line, and C_4 maroon line (upper curve). (f) Fixed nuclei: $|c_{8k}(t)|^2$, $k = 6$ red line, $k = 8$ blue line (lower curve), and C_8 maroon line (upper curve).

is zero because laser (A) does not excite the system in that direction. The x and y components of the dipole moment settle into a periodic oscillation after the excitation from the laser. These oscillations correspond directly to the vibrations of the atoms. The period of the change in the dipole moment matches with the stretching of atom $H1$ [see Fig. 2(b)].

After ionization of the asymmetric molecule occurs, the electron distribution around the molecule will change, caused by the dissipation of electronic energy into nuclear motion. This relaxation will also redistribute the electron density back towards regions of the molecule from which ionization affected the electron density the most.

The time-dependent dipole oscillations are very similar for the three lasers and the other results are not shown here.

C. Electronic coherence

To study the coherence in the electronic dynamics after ionization, we have calculated the time-dependent projections defined in Eq. (9). Figure 4 shows selected squared inner products for laser (A), elucidating pronounced coherence between various electronic states. We note that we have carried out calculations for C_2H_4 for laser (A) and no significant coherent superposition was found, and the molecular states maintain their character. In the case of C_2H_4, the amplitudes of the squared inner products remain below 0.05 and the nuclear motion has no noticeable effect. This shows the important role of asymmetry due to the replacement of a H atom with a Br atom in vinyl bromide. The bromine atom is much larger than a H atom, and there are orbitals that are more localized around the bromine atom, as compared to the delocalized orbitals in C_2H_2.

Figure 4 shows four coherent superpositions. The first [Fig. 4(a)] is between orbital 1 and 2. These two orbitals are very similar (see Fig. 1); the only difference is the nodal plane perpendicular to the C-Br axis in the case of orbital 2. These are the lowest-lying states close in energy and crossing each other's energy curve [Fig. 3(a)] several times.

Orbitals 3, 4, and 5 are grouped together closely in energy [Fig. 3(a)], crossing in energy frequently. Figure 4(b) shows the superposition of these three states (see Fig. 1 for their shape). Orbitals 3 and 4 are similar, with two hydrogens and the Br atom connected by the same phase. Orbital 5 is different from orbitals 3 and 4, having a nodal plane between the C and Br atoms.

The remaining four states, i.e., orbitals 6–9, are close in energy after ionization, but their orbitals densities are different. The coherence between orbitals 6 and 8 and between orbitals 7 and 9 is shown in Figs. 4(c) and 4(d), respectively. The shape of orbitals 7 and 9 (see Fig. 1) is distinctively different from other orbitals having the xy plane as a nodal plane. The difference between orbitals 7 and 9 is that orbital 9 has a nodal plane between the C and Br atoms.

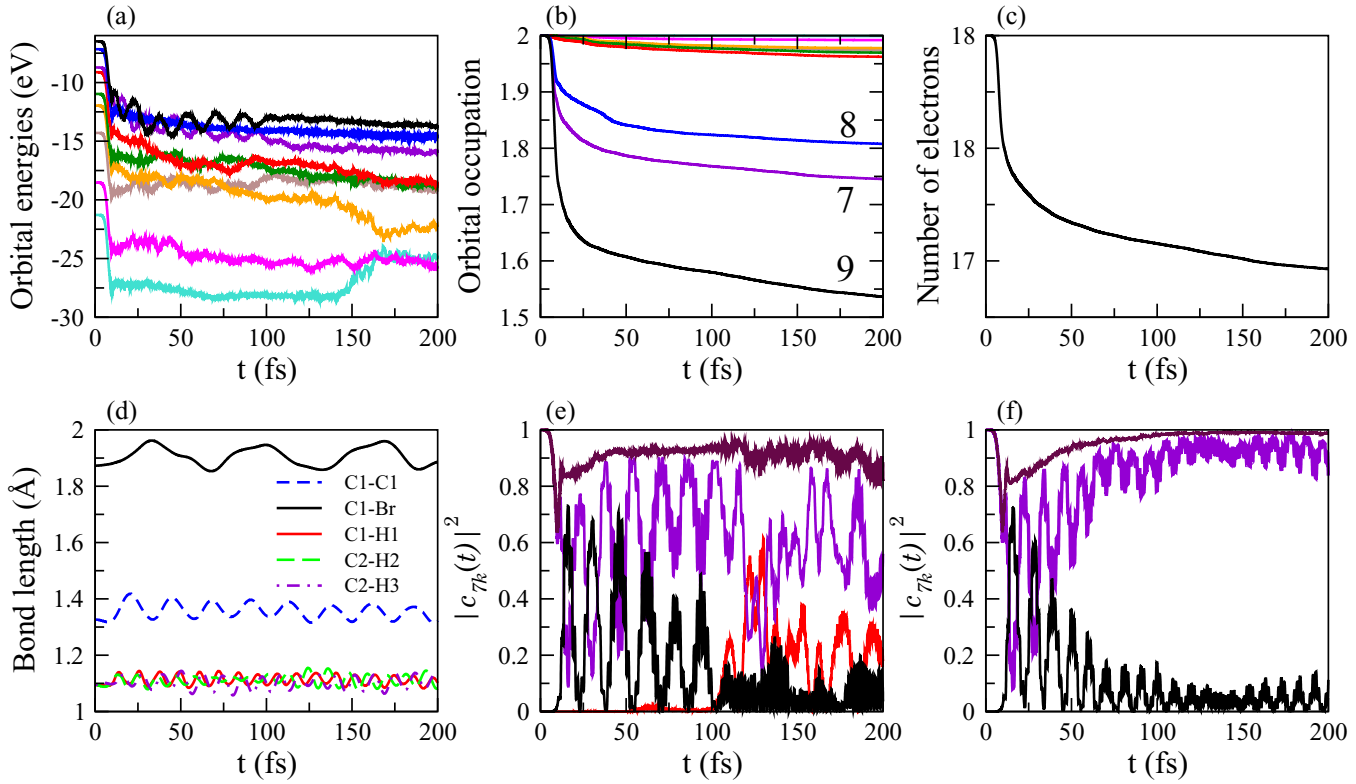

FIG. 5. (a) Orbital energies, (b) orbital occupation, (c) number of electrons, and (d) bond length between the atoms. (e) Squared inner products $|c_{7k}(t)|^2$, $k = 7$ violet line (starting at the left upper corner), $k = 9$ black line (starting at the left bottom), $k = 6$ red line, and C_7 maroon line (upper curve). (f) Squared inner products *for fixed nuclei* $|c_{7k}(t)|^2$, $k = 7$ violet line, $k = 9$ black line, and C_7 maroon line, as a function of time for laser (B). (a) The HOMO is the highest curve (orbital 9) followed by the HOMO-1 (orbital 8), and so on. (b) The indices are shown for orbitals 7–9, and the rest of the orbitals follow the order 1–6 starting from the top.

As the nodal plane of orbitals 7 and 9 is parallel to the laser field, these orbitals are less ionized than the orbitals with similar energies and the laser couples them to a lesser degree, leading to smaller coherence than in the other cases [Fig. 4(d)]. By increasing the strength of laser (A), these orbitals will be more ionized, leading to an increase of the C-Br bond length and much stronger coherence between orbitals 7 and 9. But a stronger field will eventually cause the dissociation of the molecule.

By using a perpendicular laser field [laser (B)], the most pronounced coherence is between states 7 and 9 (see Fig. 5). This is expected because these two states have a nodal plane perpendicular to the direction of the laser. After about one-hundred fs, a third state, $j = 6$, also becomes important. Orbital 6 has a nodal plane on the bromine atom and is also localized more on the ethylenyl part, so its mixing with orbitals 7 and 9 gives them some polarization either towards or away from the bromine atom.

We have repeated the calculation for laser pulse (C), which has a longer wavelength, and we have to use a stronger electric field to remove two electrons. As shown in Fig. 6, this stronger pulse ionizes the orbitals more abruptly than the 124 nm pulses. The orbital ionization is also significantly changed; the HOMO orbital is ionized the most and the electron loss of HOMO-1 is much less. The most pronounced coherence occurs between orbitals 7 and 9.

Next we investigate what happens if we instantaneously remove one electron from orbital 9 (the HOMO) or from orbital 8 (the HOMO-1). Note that the molecular plane is a nodal plane of orbital 9 (see Fig. 1), and both orbitals 8 and 9 have a nodal plane perpendicular to the C-Br axis, with similar (but 90 degrees rotated) electron density on the Br. Removing an electron corresponds to a very short, well-designed laser pulse that acts so quickly that the rest of the system has no time to react and remains frozen. Figure 7 shows that removing an electron from orbital 9 (the HOMO) causes strong vibration between C and Br, while removing an electron from orbital 8 (the HOMO-1) leads to almost no vibration between C and Br.

Removing an electron from orbital 9 (the HOMO) excites a coherent electronic oscillation between orbitals 1 and 2. Other lower orbitals up to orbital 6 show slight coupling; the coherence between higher-lying orbitals is not significant.

Removing an electron from orbital 8 (the HOMO-1) generates coherent states for both the lower- and the higher-lying orbitals. Figure 7(d) shows the time evolution of the inner product for orbital 7 into a superposition of states 7 and 9. The coherent states formed by lower-lying orbitals are somewhat similar to those that laser (A) produced (see Fig. 4). This is reasonable because laser (A) mainly ionizes orbital 8. For example, the coherence between states 1 and 2 after removing orbital 8 [Fig. 8(a)] is very much the same as the effect of

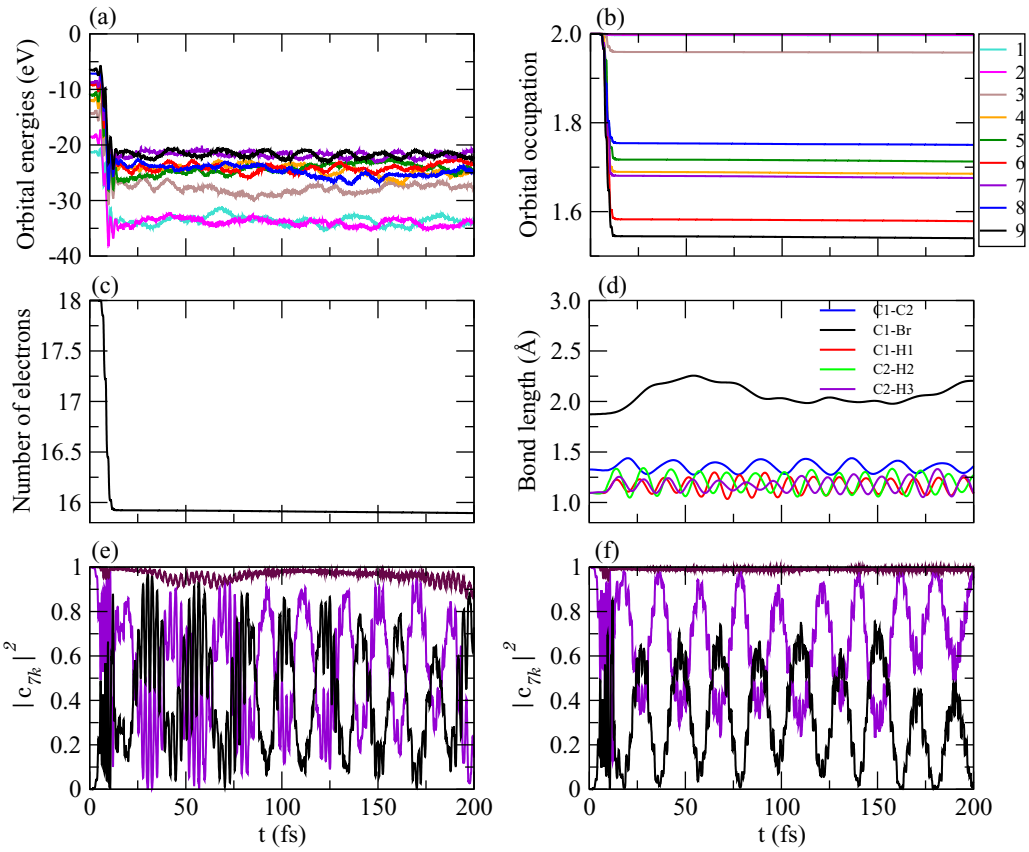

FIG. 6. (a) Orbital energies, (b) orbital occupation, (c) number of electrons, and (d) bond length between the atoms. (e) Squared inner products $|c_{7k}(t)|^2$, $k = 7$ violet line, $k = 9$ black line (starting at left bottom), and C_7 maroon line (upper curve). (f) Squared inner products *for fixed nuclei* $|c_{7k}(t)|^2$, $k = 7$ violet line, $k = 9$ black line, and C_7 maroon line, as a function of time for laser (C). (a) The HOMO is the highest curve (orbital 9) followed by the HOMO-1 (orbital 8), and so on. (b) The orbitals follow the order 1, 2, 3, 8, 5, 4, 7, 6, 9 starting from the top. Orbitals 1 and 2 are not ionized and are on top of each other.

laser (A) in Fig. 4(a). The coherence between orbitals 6 and 8 [Fig. 8(b)] is not exactly the same as Fig. 4(c), but there is some similarity at least in the strong coupling between the same states.

To explore the effect of nuclear motion, we have also performed calculations for fixed nuclei. Comparing the ionization for fixed and moving nuclei, we have found that the nuclear motion hardly affects the ionization. This is reasonable as the duration of the ionizing field is very short.

Figure 4 shows the squared inner products for laser (A), from two separate calculations, i.e., one with nuclear motion and one without nuclear motion, where the laser excites the electron dynamics only. In these cases, we also see complex coherent oscillations between different states. Comparing the moving and the fixed nuclei case, we can conclude that the nuclear motion has a profound effect on the coherence since the squared inner products and the nature of the curves is completely different.

As we have mentioned before, for an x-direction laser field, the correlation between orbitals 9 and 7 (the HOMO and HOMO-2) is very sensitive to the C-Br bond length. This is further corroborated with the fixed nuclei study: there are no coherent oscillations between these two states if the nuclear motion is not allowed [the result is not shown; the $C_{79}(t)$ is zero].

It is particularly interesting to compare the moving and fixed nuclei case for the perpendicular field [see Figs. 5(e) and 5(f)]. The two correlations start out almost identically during the expansion of the C-Br bond (up to about 35 fs), but then when the C-Br distance starts to decrease and continues to vibrate, the squared inner products deviate significantly. The electronic coherence for the fixed nuclei case diminishes, while nuclear motion causes a coherence with a third orbital.

In the case of laser pulse (C), as Figs. 6(e) and 6(f) show, the coherence between orbitals 7 and 9 is only slightly affected by the nuclear motion. This is quite the opposite of what we have observed in the case of laser (A), where the coherence was caused by the nuclear motion. Note, however, that in this case, the HOMO (orbital 9) and not the HOMO-1 orbital was ionized most, the C1-C2 motion is smoother and more sinusoidal, and the amplitude of the C-H motions is smaller in the case of laser (C) than in the case of the other x-direction excitation, laser (A).

One can also visualize the electronic coherence by taking snapshots of the electron dynamics. Figure 9 shows snapshots of charge density and the change in the charge density on a 0.5 fs timescale. The density oscillates rapidly around the bromine and between the carbon atoms. The timescale of this charge migration is very short, so it corresponds to a sharp change in the inner products. This sudden change of

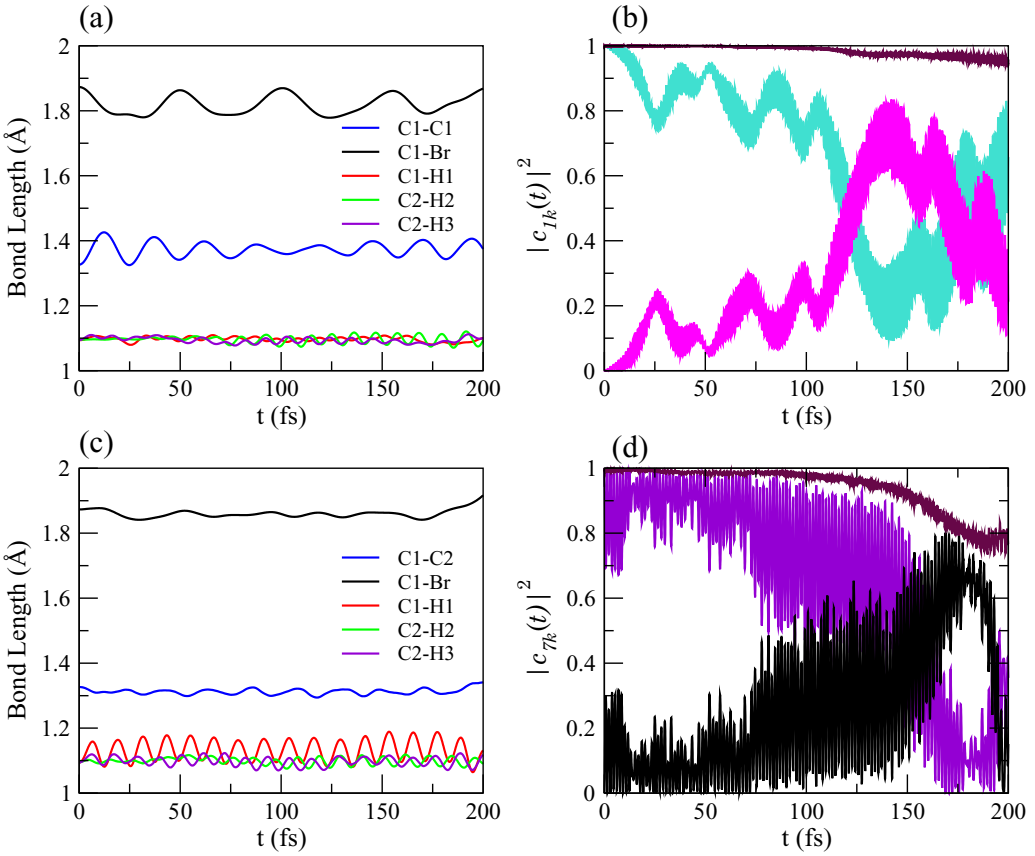

FIG. 7. (a),(c) Bond lengths. (b) Squared inner products $|c_{1k}(t)|^2$, $k = 1$ cyan line, $k = 2$ magenta line (starting at left bottom), and C_1 maroon line (upper curve), when one electron is instantaneously removed from orbital 9 (the HOMO). (d) Squared inner products $|c_{7k}(t)|^2$, $k = 7$ violet line (starting at left bottom), $k = 9$ black line, and C_7 maroon line (upper curve), when one electron is instantaneously removed from orbital 8 (the HOMO-1).

the inner product explains the rapid oscillations in Figs. 4–8. Also shown in Fig. 9 is the current density, which helps the interpretation of the change in charge density, proving that the density oscillates around the bromine atom.

At a later time (see Fig. 10), quite a different picture emerges. The density fluctuations are not as centered around the Br atom, though they are still present around the Br. At this time, the density fluctuates around the carbon-hydrogen bonds. Also, at some points in time, the regions of positive and negative flux become larger and more delocalized. The density fluctuations around the H atoms are mostly due to the nuclear motion. The bond length rapidly changes (about 0.05–0.15 Å/fs) even on the subfemtosecond time frame.

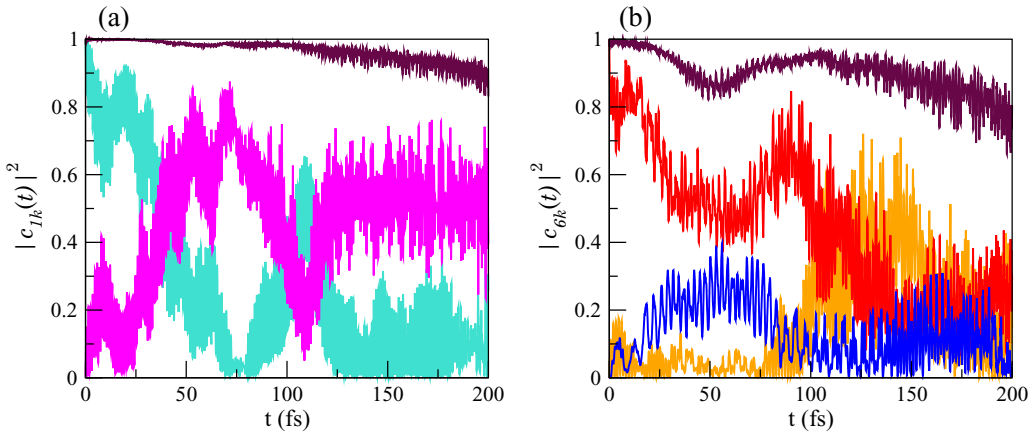

FIG. 8. Squared inner products when one electron is instantaneously removed from orbital 8 (the HOMO-1). (a) $|c_{1k}(t)|^2$, $k = 1$ cyan line, $k = 2$ magenta line (starting at left bottom), and C_1 maroon line (upper curve). (b) $|c_{6k}(t)|^2$, $k = 6$ red line (starting at left top), $k = 4$ orange line (light gray), $k = 8$ blue line (starting at left bottom), and C_6 maroon line (upper curve).

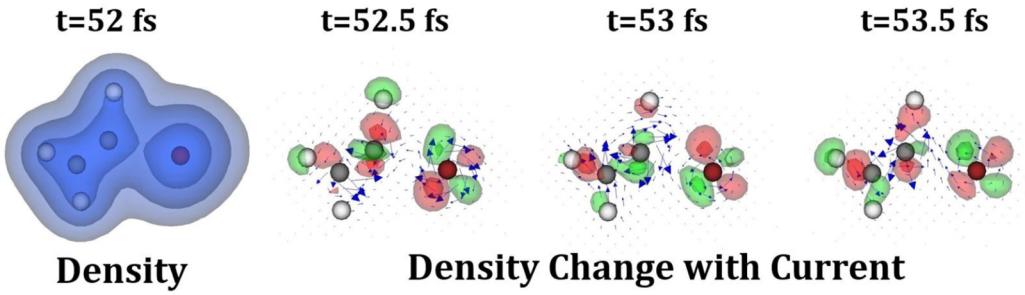

FIG. 9. Snapshots of the electron density isosurfaces (blue with values of 0.5, 0.05, and 0.005) at 52 fs and the subsequent change to the density at 52.5, 53, and 53.5 fs (green with values of 0.1 and 0.033 and red with values of −0.033 and −0.1). Red values indicate areas where electron density has decreased and green values indicate areas where electron density has increased. The electron current density at each point is also shown.

IV. SUMMARY

Short-time oscillations due to electron dynamics and nuclear motion have been studied in the molecule vinyl bromide with TDDFT. Vinyl bromide is an ideal system for the study of electron coherence because the molecule has two distinct portions, i.e., the bromide atom and the carbon-hydrogen part (ethylenyl fragment), with ground-state orbitals that tend to localize more on one or the other. Instantaneously removing an electron from a given orbital causes electron density rearrangement and coherent oscillations in some orbitals, but not in others.

The common property of these coherent oscillations is the presence of short-time oscillations, i.e., tens of attoseconds, superposed on a longer-range (tens of fs) oscillation. The longer oscillation period can be explained by the energy difference (1 eV corresponds to 4 fs) between the orbitals. The short-time oscillations are due to the laser excitation of the orbitals and initially follow the period of the laser. The interaction between the electrons couples the oscillations and short-time irregular beats appear.

Different laser parameters and alignments produced coherent oscillations, but the details of the electron and nuclear dynamics is very sensitive to the laser. A slight change in the laser intensity can change the bond length and lead to dissociation, and the nuclear motion can destroy or induce electron coherence. A different alignment or different wavelength can significantly change the ionization of a given orbital compared to others, irrespective of the ground-state energies.

Despite the fact that different orbitals are ionized to different extents and the ionization is followed by a large-amplitude nuclear vibrational motion, the ground-state molecular orbitals preserve their character and the excitation leads to coherence between specific states only. By choosing a laser alignment depending on the symmetry of the molecular states, specific orbitals can be ionized, which may lead to controlled generation of coherent excitation in molecules.

Comparing the coherence calculated with and without nuclear motion, one can see that the main effect of the nuclear dynamics is the enhancement of coherence. The nuclear motion changes the overlap between the ground state with the time-propagated molecular orbitals increasing and decreasing the coupling between them. This leads to higher-amplitude oscillation in the occupation of the coupled states. The calculations also show that nuclear motion modulates the dipole

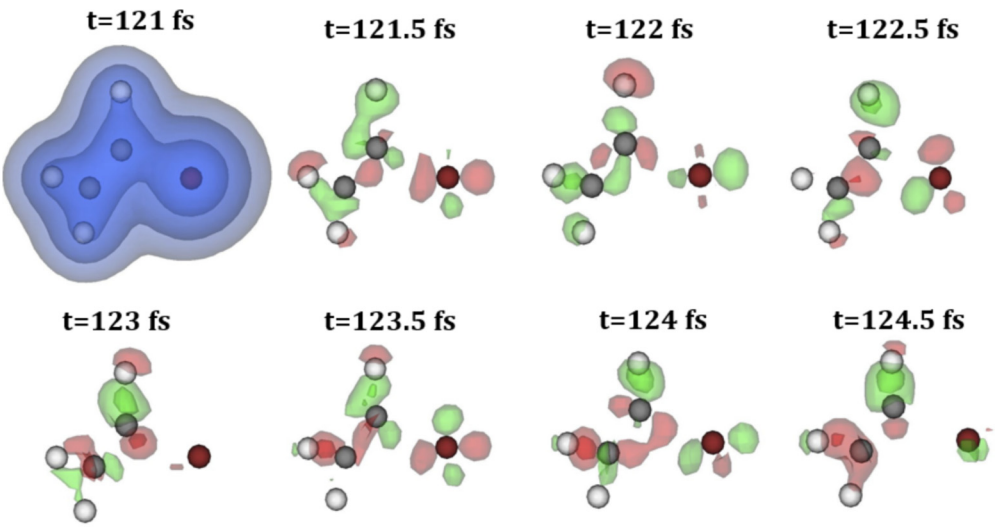

FIG. 10. Snapshots of the electron density isosurfaces (blue with values of 0.5, 0.05, and 0.005) at 121 fs and the subsequent change to the density (green with values of 0.1 and 0.033 and red with values of −0.033 and −0.1) at 0.5 fs increments.

moment and the time dependence of the energy, but the effect of nuclear motion is less noticeable on the coherent oscillation since the time dependence of the oscillations is very similar in the moving and frozen nuclei case. The strong effect of nuclear motion on electron coherence and charge transfer was also shown by a combined experimental and theoretical study [60] of a prototypical artificial light-harvesting system.

Over time, the electronic excitation is expected to decay into nuclear motion and possibly fragmentation of the molecule. In the case of ionization of vinyl bromide, the occupied and the lowest unoccupied molecular orbital (LUMO) states are energetically well separated. The excitation couples certain occupied molecular orbitals and the decay to nuclear motion is slow. This maintains a long-lived coherence between electronic states, making the vinyl bromide a good candidate for experimental studies of electronic coherence in molecules.

Ehrenfest dynamics, combined with TDDFT or other approaches to describe the electronic motion, is often used to describe the ultrafast dynamics in molecules [2,33,52–55,61]. Ehrenfest dynamics has recently been extended to fully quantum nuclear motion [32,32]. This, along with other emerging quantum nuclear calculations [27,28], will allow the evaluation of the influence of the nuclear quantum nature on the electronic coherence. The charge oscillation of the excited states in vinyl bromide ions is mainly due to the superposition of the localized orbitals of the bromine and ethylenyl fragments, and the study of the effect of quantum nuclear dynamics would be very interesting for the full assessment of the coherence. Such a study, however, is computationally not feasible yet in the TDDFT framework.

ACKNOWLEDGMENT

H.D. was funded by the research Scientific Research Plan Projects of Shaanxi Education Department, China (Grant No. 16JK1384).

[1] P. M. Kraus, B. Mignolet, D. Baykusheva, A. Rupenyan, L. Horný, E. F. Penka, G. Grassi, O. I. Tolstikhin, J. Schneider, F. Jensen, L. B. Madsen, A. D. Bandrauk, F. Remacle, and H. J. Wörner, Science **350**, 790 (2015).

[2] H. J. Wörner, C. A. Arrell, N. Banerji, A. Cannizzo, M. Chergui, A. K. Das, P. Hamm, U. Keller, P. M. Kraus, E. Liberatore, P. Lopez-Tarifa, M. Lucchini, M. Meuwly, C. Milne, J.-E. Moser, U. Rothlisberger, G. Smolentsev, J. Teuscher, J. A. van Bokhoven, and O. Wenger, Struct. Dyn. **4**, 061508 (2017).

[3] T. Brabec and F. Krausz, Rev. Mod. Phys. **72**, 545 (2000).

[4] P. B. Corkum and F. Krausz, Nat. Phys. **3**, 381 (2007).

[5] E. Goulielmakis, Z.-H. Loh, A. Wirth, R. Santra, N. Rohringer, V. S. Yakovlev, S. Zherebtsov, T. Pfeifer, A. M. Azzeer, M. F. Kling, S. R. Leone, and F. Krausz, Nature (London) **466**, 739 (2010).

[6] M. F. Kling, C. Siedschlag, A. J. Verhoef, J. I. Khan, M. Schultze, T. Uphues, Y. Ni, M. Uiberacker, M. Drescher, F. Krausz, and M. J. J. Vrakking, Science **312**, 246 (2006).

[7] F. Krausz and M. Ivanov, Rev. Mod. Phys. **81**, 163 (2009).

[8] L. Cattaneo, J. Vos, R. Y. Bello, A. Palacios, S. Heuser, L. Pedrelli, M. Lucchini, C. Cirelli, F. Martín, and U. Keller, Nat. Phys. **14**, 733 (2018).

[9] R. Hildner, D. Brinks, and N. F. van Hulst, Nat. Phys. **7**, 172 (2010).

[10] G. S. Engel, T. R. Calhoun, E. L. Read, T.-K. Ahn, T. Mancal, Y.-C. Cheng, R. E. Blankenship, and G. R. Fleming, Nature (London) **446**, 782 (2007).

[11] E. Collini, C. Y. Wong, K. E. Wilk, P. M. G. Curmi, P. Brumer, and G. D. Scholes, Nature (London) **463**, 644 (2010).

[12] D. Hayes, G. B. Griffin, and G. S. Engel, Science **340**, 1431 (2013).

[13] T. D. Ladd, F. Jelezko, R. Laflamme, Y. Nakamura, C. Monroe, and J. L. O'Brien, Nature (London) **464**, 45 (2010).

[14] I. Buluta and F. Nori, Science **326**, 108 (2009).

[15] O. Smirnova, Y. Mairesse, S. Patchkovskii, N. Dudovich, D. Villeneuve, P. Corkum, and M. Y. Ivanov, Nature (London) **460**, 972 (2009).

[16] K. Hosaka, H. Shimada, H. Chiba, H. Katsuki, Y. Teranishi, Y. Ohtsuki, and K. Ohmori, Phys. Rev. Lett. **104**, 180501 (2010).

[17] M. P. A. Branderhorst, P. Londero, P. Wasylczyk, C. Brif, R. L. Kosut, H. Rabitz, and I. A. Walmsley, Science **320**, 638 (2008).

[18] Y. Kobayashi, M. Reduzzi, K. F. Chang, H. Timmers, D. M. Neumark, and S. R. Leone, Phys. Rev. Lett. **120**, 233201 (2018).

[19] A. Wirth, R. Santra, and E. Goulielmakis, Chem. Phys. **414**, 149 (2013).

[20] H. Hennig, J. Breidbach, and L. S. Cederbaum, J. Chem. Phys. **122**, 134104 (2005).

[21] S. Pabst, M. Lein, and H. J. Wörner, Phys. Rev. A **93**, 023412 (2016).

[22] N. Rohringer and R. Santra, Phys. Rev. A **79**, 053402 (2009).

[23] M. Lara-Astiaso, A. Palacios, P. Decleva, I. Tavernelli, and F. Martín, Chem. Phys. Lett. **683**, 357 (2017).

[24] D. B. Lingerfelt, P. J. Lestrange, J. J. Radler, S. E. Brown-Xu, P. Kim, F. N. Castellano, L. X. Chen, and X. Li, J. Phys. Chem. A **121**, 1932 (2017).

[25] K.-J. Yuan and A. D. Bandrauk, Phys. Chem. Chem. Phys. **19**, 25846 (2017).

[26] V. Despré, N. V. Golubev, and A. I. Kuleff, Phys. Rev. Lett. **121**, 203002 (2018).

[27] C. Arnold, O. Vendrell, and R. Santra, Phys. Rev. A **95**, 033425 (2017).

[28] M. Vacher, M. J. Bearpark, M. A. Robb, and J. P. Malhado, Phys. Rev. Lett. **118**, 083001 (2017).

[29] R. Santra, V. S. Yakovlev, T. Pfeifer, and Z.-H. Loh, Phys. Rev. A **83**, 033405 (2011).

[30] J. J. Rørstad, N. S. W. Ravn, L. Yue, and L. B. Madsen, Phys. Rev. A **98**, 053401 (2018).

[31] A. Trabattoni, M. Galli, M. Lara-Astiaso, A. Palacios, J. Greenwood, I. Tavernelli, P. Decleva, M. Nisoli, F. Martín, and F. Calegari, Philos. Trans. R. Soc., A **377**, 20170472 (2019).

[32] A. J. Jenkins, K. E. Spinlove, M. Vacher, G. A. Worth, and M. A. Robb, J. Chem. Phys. **149**, 094108 (2018).
[33] F. Calegari, D. Ayuso, A. Trabattoni, L. Belshaw, S. De Camillis, S. Anumula, F. Frassetto, L. Poletto, A. Palacios, P. Decleva, J. B. Greenwood, F. Martín, and M. Nisoli, Science **346**, 336 (2014).
[34] E. Runge and E. K. U. Gross, Phys. Rev. Lett. **52**, 997 (1984).
[35] S. Bubin, M. Atkinson, K. Varga, X. Xie, S. Roither, D. Kartashov, A. Baltuška, and M. Kitzler, Phys. Rev. A **86**, 043407 (2012).
[36] A. Russakoff, S. Bubin, X. Xie, S. Erattupuzha, M. Kitzler, and K. Varga, Phys. Rev. A **91**, 023422 (2015).
[37] X. Xie, S. Roither, M. Schöffler, H. Xu, S. Bubin, E. Lötstedt, S. Erattuphuza, A. Iwasaki, D. Kartashov, K. Varga, G. G. Paulus, A. Baltuška, K. Yamanouchi, and M. Kitzler, Phys. Rev. A **89**, 023429 (2014).
[38] S. Bubin and K. Varga, Phys. Rev. B **85**, 205441 (2012).
[39] S. Bubin and K. Varga, Appl. Phys. Lett. **98**, 154101 (2011).
[40] S. Bubin and K. Varga, J. Appl. Phys. **110**, 064905 (2011).
[41] S. Bubin, B. Wang, S. Pantelides, and K. Varga, Phys. Rev. B **85**, 235435 (2012).
[42] J.-A. Yan, J. A. Driscoll, B. K. Wyatt, K. Varga, and S. T. Pantelides, Phys. Rev. B **84**, 224117 (2011).
[43] J. P. Perdew and A. Zunger, Phys. Rev. B **23**, 5048 (1981).
[44] N. Troullier and J. L. Martins, Phys. Rev. B **43**, 1993 (1991).
[45] G. F. Bertsch, J.-I. Iwata, A. Rubio, and K. Yabana, Phys. Rev. B **62**, 7998 (2000).
[46] J.-I. Iwata, K. Yabana, and G. F. Bertsch, J. Chem. Phys. **115**, 8773 (2001).
[47] K. Yabana and G. F. Bertsch, Phys. Rev. A **60**, 1271 (1999).
[48] K. Yabana and G. F. Bertsch, Phys. Rev. B **54**, 4484 (1996).
[49] K. Varga and J. A. Driscoll, *Computational Nanoscience* (Cambridge University Press, New York, 2011).
[50] A. Castro, M. A. L. Marques, and A. Rubio, J. Chem. Phys. **121**, 3425 (2004).
[51] D. E. Manolopoulos, J. Chem. Phys. **117**, 9552 (2002).
[52] I. Polyak, A. J. Jenkins, M. Vacher, M. E. F. Bouduban, M. J. Bearpark, and M. A. Robb, Mol. Phys. **116**, 2474 (2018).
[53] M. Vacher, M. J. Bearpark, and M. A. Robb, J. Chem. Phys. **140**, 201102 (2014).
[54] M. Vacher, D. Mendive-Tapia, M. J. Bearpark, and M. A. Robb, J. Chem. Phys. **142**, 094105 (2015).
[55] D. Mendive-Tapia, M. Vacher, M. J. Bearpark, and M. A. Robb, J. Chem. Phys. **139**, 044110 (2013).
[56] S. Kümmel, Adv. Energy Mater. **7**, 1700440 (2017).
[57] N. T. Maitra, J. Chem. Phys. **144**, 220901 (2016).
[58] N. T. Maitra, J. Phys.: Condens. Matter **29**, 423001 (2017).
[59] M.-F. Lin, D. M. Neumark, O. Gessner, and S. R. Leone, J. Chem. Phys. **140**, 064311 (2014).
[60] C. Andrea Rozzi, S. Maria Falke, N. Spallanzani, A. Rubio, E. Molinari, D. Brida, M. Maiuri, G. Cerullo, H. Schramm, J. Christoffers, and C. Lienau, Nat. Commun. **4**, 1602 (2013).
[61] M. Vacher, J. Meisner, D. Mendive-Tapia, M. J. Bearpark, and M. A. Robb, J. Phys. Chem. A **119**, 5165 (2015).